Magneto-optical studies of the $Z_{1,2}$ exciton-polaritons in CuI: Effects of finite exciton wave vector

S. Suga
The Institute for Solid State Physics, The University of Tokyo, Roppongi, Minato-ku, Tokyo, Japan and Max-Planck-Institut für Festkörperforschung, 7000 Stuttgart 80, Federal Republic of Germany

K. Cho
Faculty of Engineering Science, Osaka University, Toyonaka, Osaka, Japan and Max-Planck-Institut für Festkörperforschung, 7000 Stuttgart 80, Federal Republic of Germany

Y. Niji
Faculty of Engineering Science, Osaka University, Toyonaka, Osaka, Japan

J. C. Merle
Université Louis Pasteur, Laboratoire de Spectroscopie et d'Optique du Corps Solide, 5 Rue de l'Université, 67084 Strasbourg Cedex, France

T. Sauder
Université de Nancy-Metz, Laboratoire de Physique des Milieux Condensés, Ile du Saulcy 57000 Metz, France
(Received 24 July 1979)

Polarization-resolved magnetoreflectance spectra associated with the $Z_{1,2}$ ($\Gamma_8\times\Gamma_6$) exciton states in CuI are measured up to 12 T. The appearance and the anisotropic Zeeman splitting of the reflectance anomaly originating from the (Γ_4,Γ_3) exciton states are interpreted by means of the "k-linear term effect" on the $Z_{1,2}$ excitons in zinc-blende crystals. According to a recent theory which treats the reflectance line shape due to multicomponent polaritons, the measured results are quantitatively analyzed, providing the values of exciton parameters such as $\tilde{\kappa}$, $\tilde{g}_c$, γ_2^{ex}, $\hbar K_l$, and exchange interactions. Magnetoluminescence spectra measured in the $Z_{1,2}$ excitons region and their unusual temperature change are well understood in this model which explains the contributions of the (Γ_4,Γ_3) exciton polaritons to the normally observable Γ_5 lower and upper polariton luminescence bands.

PACS numbers: 71.36. + c, 71.70.Gm, 78.20.Ls, 78.55.Hx

I. INTRODUCTION

The internal structure of degenerate exciton states in semiconductors and insulators has been extensively investigated recently by use of external perturbations such as uniaxial stress and electric field or magnetic field, and band parameters as well as details of the electron-hole interactions have been evaluated in a wide variety of cases.[1] For example, magnetoreflectance studies on GaAs and InP (Ref. 2) enabled one to resolve six Zeeman components of the eightfold-degenerate ground exciton states, which were quantitatively analyzed according to a degenerate perturbation theory.[3] Within various zinc-blende crystals, some substances were known to show a reflectance anomaly associated with the exciton ground states even without any external perturbation. In the case of CuBr,[4] magnetic circular reflectance (MCR) as well as magnetic circular polarization of luminescence (MCP) were measured to investigate the origin of the anomalous reflectance spike of the $Z_{1,2}$ exciton states. Magnetoreflectance measurement on cleaved {110} surfaces of CdTe, which also displayed a similar reflectance anomaly, revealed all the eight Zeeman components with well-defined polarizations.[5] In both cases of CuBr and CdTe, the reflectance anomaly was well understood as due to the k-linear term effect of the Γ_8 valence band coupled with the finite exciton wave vector $\vec{K}$.

Detailed knowledge about the internal structure of degenerate exciton states is more and more required nowadays, in order to understand, for example, biexciton (excitonic molecule) and polariton states. The aim of the present work is to investigate both the reflectance and luminescence spectra due to the eightfold-degenerate $Z_{1,2}$ excitons in CuI under a high magnetic field and quantitatively estimate exciton parameters through reflectance line-shape analysis. The optical spectra of CuI are satisfactorily interpreted as resulting from the effects of the finite exciton wave vector on the $Z_{1,2}$ exciton polariton states as well as of the electron-hole exchange interactions.

II. EXPERIMENTAL

We have measured normal incidence reflectance and luminescence spectra of the $Z_{1,2}$ exciton polaritons from a {110} cleaved surface of CuI made by the traveling solvent technique.[6] A Xe discharge lamp and a 3250-Å line (5 mW) of a He-Cd laser

were used as light sources for reflectance and luminescence measurements, respectively. The specular reflectance from a large cleaved surface with a dimension of about 10×10 mm^2 enabled us to measure detailed structures of the reflectance spectrum with a good signal-to-noise ratio even though the sample was placed at the center of a deep bore of magneto-optical cryostat considerably away from the Xe lamp and a monochromator as shown in Fig. 1. The sample mounted at the top of the sample holder was inserted into an inner wall of a helium flow exchange gas cryostat and cooled down to about 4.5 K by convection of the helium exchange gas. The sample temperature could be changed to an arbitrary degree by regulating the flow rate of the liquid helium through the cryostat. The sample could be changed easily by extracting the whole sample holder outside, while blowing dry helium gas within the cryostat inner wall in order to protect the cold window at the top of the cryostat from gas condensation. The whole cryostat was placed in a horizontal vacuum bore surrounded by a 12.6-T Nb_3Sn superconducting solenoid.

The set up shown in Fig. 1 corresponds to the Faraday configuration with the photon wave vector parallel to the magnetic field $\vec{H}$. In order to analyze the circular polarization of the reflected or luminescent light, a quarter-wave plate in combination with a linear polarizer was placed just in front of the entrance slit of a $\frac{3}{4}$-m Spex single-grating monochromator attached with a cooled photomultiplier. As a quarter-wave plate, we employed a Morvue PEM-3 photoelastic quartz modulator driven by 50 kHz. The excitation light was mechanically chopped at 1 kHz. The output of the photomultiplier was fed into two lock-in amplifiers in order to measure both the mean value and the difference of the two circularly polarized spectra. The latter, not divided by the former, corresponds to MCR and MCP spectra shown in the present paper. The notations of σ_{+1} and σ_{-1} correspond to the circularly polarized lights which excite the $M_J=+1$ and $M_J=-1$ states of the $J=1$ exciton, respectively. Insofar as the Zeeman splitting is linear in the magnetic field, the effective g value of the exciton is defined by $[E(\sigma_{+1})-E(\sigma_{-1})]/\mu_B H$, where E are the resonance energies of the exciton Zeeman components. The magnitude of the difference spectrum was calibrated by a steady circular polarizer set before the modulating quarter-wave plate. In order to measure the magneto-optical spectra in the Voigt configuration with the photon wave vector perpendicular to $\vec{H}$, we only required another sample holder with an aluminum mirror, 45 degrees inclined with respect to $\vec{H}$, and a sample setting table parallel to $\vec{H}$. The resolution of the monochromator was typically set to 0.3 and 1 Å for reflectance and luminescence measurements, respectively.

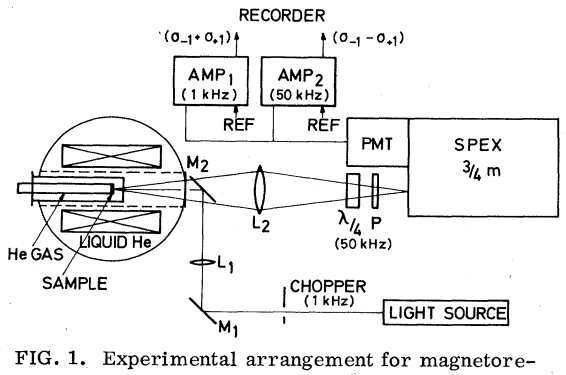

FIG. 1. Experimental arrangement for magnetoreflectance and luminescence measurements. M and L indicate mirrors and lenses, respectively. $\lambda/4$ represents a quarter-wave plate which functions as a circular analyzer in combination with a linear polarizer P. On the left side is shown a horizontal cross section of the helium flow exchange gas cryostat placed in a superconducting solenoid.

III. RESULTS

A. Reflectance and MCR

The reflectance spectrum of the $Z_{1,2}$ excitons in CuI is composed of a main broad reflectance band and an anomalous sharp spike on its low-energy shoulder.[7] This reflectance spike is generally observable on good crystal surfaces, such as cleaved surfaces of bulk crystals made by the Bridgman method or by the traveling-solvent technique. In order to ascertain the origin of this structure, an external magnetic field is applied. Figure 2 shows the result of MCR at several magnetic fields measured in the Faraday configuration with $\vec{K}||\vec{H}||[110]$. The direct reflectance spectra (solid lines) show a clear doublet splitting of the anomalous spike under the action of the magnetic field. The corresponding MCR spectra show peaks in this energy region. By comparing the MCR spectra with the polarization-resolved spectra shown in the insert at the bottom, one notices that each component of the Zeeman doublet is completely polarized. From the energy separation of the reflectance minima just on the high-energy side of each spike in the σ_{-1} and σ_{+1} spectra at 12 T, we evaluate the effective g value of the excitons responsible for the reflectance spike to be -1.8 ± 0.1. Here we have taken the energy positions of reflectance minima of the anomalous spike instead of maxima, because the exciton resonance energies are very close to the former according to line-shape analysis. The data at 6 T give a g value in close agree-

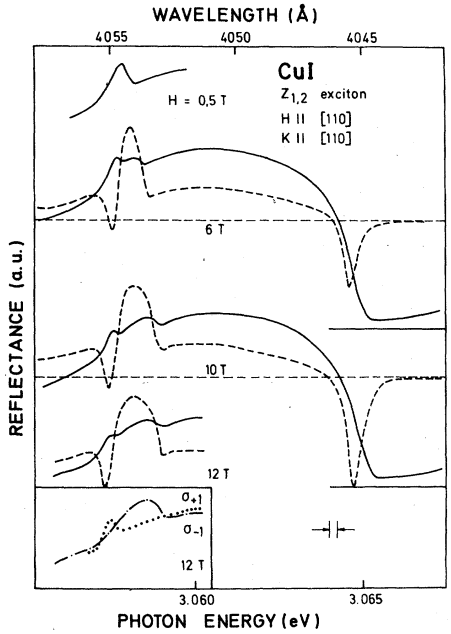

FIG. 2. Reflectance (solid lines) and MCR (dashed) spectra of the $Z_{1,2}$ exciton polaritons in CuI measured at 8 K in the Faraday configuration with $\vec{K} \| \vec{H} \| [110]$. The solid and dashed horizontal lines correspond to zero lines of reflectance and MCR, respectively. The inset at the bottom shows the individually polarized components [σ_{+1} (dotted) and σ_{-1} (dot-dashed)] of the anomalous reflectance spike measured by use of a steady circular analyzer.

ment with this value. The most remarkable feature of the spectral line shape of this Zeeman doublet is that the structure of the σ_{-1} component (dot-dashed line) becomes more prominent than that of σ_{+1} (dotted line) with increasing magnetic field. One can observe another MCR structure just around the high-energy edge of the main reflectance band. Since a direct splitting is hardly observable in this case, the effective g value is evaluated from an MCR line-shape analysis to be $+0.6 \pm 0.1$ on the basis of a rigid shift of the corresponding Zeeman components, comparing a derivative of the observed reflectance spectrum with the MCR spectrum.

A large {110} cleaved surface of the present CuI crystal enabled us to measure anisotropic magnetoreflectance spectra in the Voigt configuration with $\vec{K} \| [110]$ for $\vec{H} \| [1\bar{1}0]$, $\vec{H} \| [001]$, or $\vec{H} \| [1\bar{1}1]$. Figure 3 shows the $\sigma(\vec{E} \perp \vec{H})$ and $\pi(\vec{E} \| \vec{H})$ spectra of the $Z_{1,2}$ exciton reflectance at 12 T for $\vec{K} \| [110]$ and $\vec{H} \| [1\bar{1}0]$. The reflectance spike shows a doublet splitting in the σ spectrum and a broad hump in the π spectrum. This splitting of the σ doublet components at 12 T gives an absolute magnitude of the g value as 0.9 ± 0.1, which coincides with the value evaluated at 8 T. One notices the

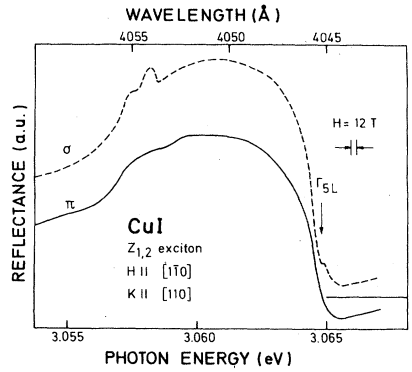

FIG. 3. Reflectance spectra of the $Z_{1,2}$ exciton polaritons in CuI at $H = 12$ T in the Voigt configuration with $\vec{K} \| [110]$ and $\vec{H} \| [1\bar{1}0]$. σ (dashed line) and π (solid) spectra correspond to the polarization with $\vec{E} \perp \vec{H}$ and $\vec{E} \| \vec{H}$, respectively.

large anisotropy of this value compared with the corresponding value (−1.8) obtained in the Faraday configuration. The other feature of this result is the appearance of an additional reflectance step in the σ spectrum at the high-energy edge of the main broad reflectance band under high magnetic fields above 8 T. This structure is assigned to the Γ_{5L} longitudinal exciton state which becomes dipole allowed due to a linear Zeeman mixing with the Γ_{5T} transverse exciton state, in a similar way as has been reported on CuCl.[8] For two other configurations with $\vec{K} \| [110]$, $\vec{H} \| [001]$ or $\vec{K} \| [110]$, $\vec{H} \| [1\bar{1}1]$, the Zeeman splitting of the anomalous reflectance spike either in σ or π spectra is so faint that one cannot quantitatively analyze the result.

B. Luminescence and MCP

Luminescence spectra of CuI are observed around the anomalous reflectance spike and at the high-energy edge of the main broad reflectance band. In Fig. 4 are shown the MCP spectra measured at 8 K in the Faraday configuration with $\vec{K} \| \vec{H} \| [110]$. Figure 5 shows the temperature change of the luminescence spectra under a magnetic field of 10 T. The luminescence band upper polariton (UP) at the highest energy provides a simple MCP spectrum under high magnetic fields, the g value of which is estimated as $+0.7 \pm 0.1$ by neglecting thermal population effect, in a similar way as described before for the MCR. In contrast, the two luminescence bands in the low-energy region display very complex MCP spectra which have unusual temperature changes as a whole. Both the luminescence spectrum and the MCP signal (composed of a pair of a maximum and a minimum) in the energy region of the B band at 3.055 eV decrease considerably with increasing temperature in comparison with the rest. In

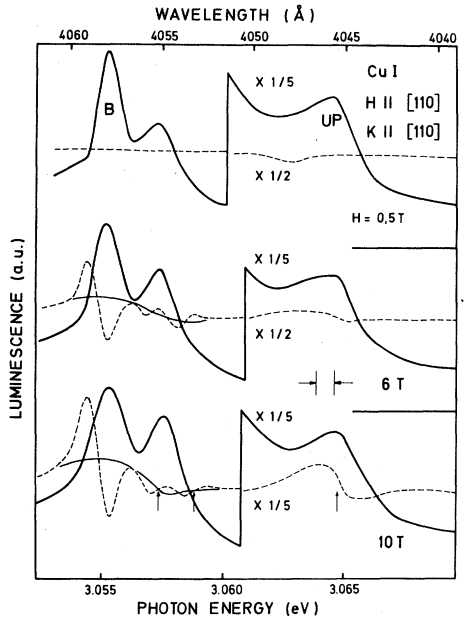

FIG. 4. Luminescence (thick solid curves) and MCP (dashed) spectra of the $Z_{1,2}$ exciton polaritons in CuI at 8 K in the Faraday configuration. B is due to a bound exciton luminescence (see text). UP is the upper polariton luminescence. The two upward arrows in the low-energy region at 10 T show the resonance energies of the polariton luminescence estimated from the MCP spectrum. The other upward arrow at 3.0648 eV indicates the energy position of the additional reflectance step shown in Fig. 3, which is assigned to the longitudinal state of the Γ_5 exciton (see text). The thin solid lines show the background MCP in the low-energy region.

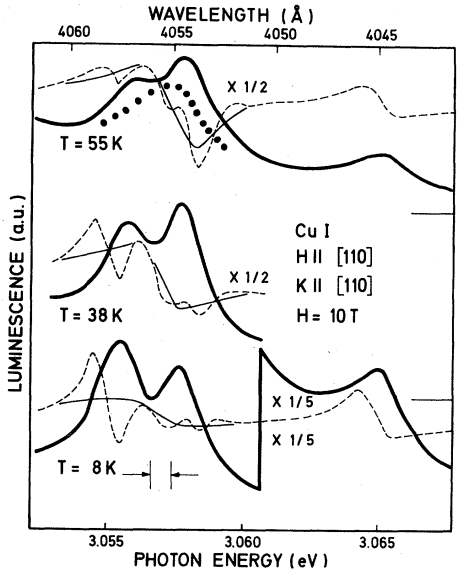

FIG. 5. Luminescence (thick solid) and MCP (dashed) spectra of the $Z_{1,2}$ exciton polaritons in CuI as a function of temperature. The multiplication factor $\times\frac{1}{2}$ only applies to the MCP spectra at 38 and 55 K. The solid thin lines show the background contribution of the Γ_5 exciton polariton to the MCP spectra in the low-energy region. The dotted line gives the contribution of the Γ_{5T} lower polariton luminescence, tentatively evaluated from the background MCP.

addition, the intensity and the line shape of the luminescence band B strongly depend upon crystals made by a different method. Therefore the band B is assigned to a bound exciton luminescence. The g value of the B band is estimated as $+0.9 \pm 0.1$ by assuming a rigid shift of two Zeeman components. In the region of the other luminescence band with a peak at 3.057 eV, two MCP structures, each composed of a negative peak on the low-energy side and a positive peak on the high-energy side providing a negative g value, are clearly resolved. The upward arrows show the resonance energies of these two MCP structures evaluated simply by assuming a rigid shift of each Zeeman component. Within this approximation, negative and positive MCP signals with roughly the same integrated intensity are expected below and above each resonance energy. The solid thin lines in Figs. 4 and 5 indicate the background MCP spectra which are obtained by subtracting these three MCP structures below 3.06 eV from experimental curves. With regard to this evaluated background MCP, one notices that the line shape, except for its amplitude, remains almost the same irrespective of temperature and the magnetic-field intensity. In addition, this line shape is very similar to that of the UP luminescence.

IV. DISCUSSIONS

A. Analysis of the reflectance spectra

For the analysis of these experimental results, we have to consider various interaction mechanisms which act among the subcomponents of the $Z_{1,2}(\Gamma_8 \times \Gamma_6)$ $1s$ excitons.[1,3] The relevant mechanisms are (a) electron-hole exchange interaction (H_{exch}), (b) Zeeman interaction (H_Z), and (c) energy terms linear (H_{K1}) and quadratic (H_{K2}) in translational wave vector $\vec{K}$. The term H_{K2} includes not only the well-known spatial (resonance) dispersion effect,[9] but also the effect of heavy- and light-mass excitons.[10] We neglect (d) the quadratic Zeeman effect and (e) the warping effect possibly included in H_{K2}. The total Hamiltonian is then written as

$$H = H_Z + H_{K1} + H_{K2} + H_{\text{exch}} .$$

The eight sublevels of the $Z_{1,2}$ $1s$ excitons are

denoted as $|J,M_J\rangle$ ($J=1$ or 2, $M_J=J,\ldots,-J$), and the quantization axis is taken along the $\langle 110\rangle$ crystallographic axis. We consider the Faraday configuration with $\vec{K}\,||\vec{H}||[110]$. In this geometry, leading terms of the Hamiltonian matrix for the $\sigma_{\pm 1}$ polarized states are represented by the following block-diagonal forms for ($|2,\mp 2\rangle$, $|2,\pm 1\rangle$, $|1,\pm 1\rangle$).[1,3,4]

$$H_Z+H_{K1}=\pm\begin{pmatrix} -\frac{1}{2}\bar{g}_c+3\bar{\kappa}+6\bar{q} & -iT & -i\sqrt{3}\,T \\ iT & \frac{1}{4}\bar{g}_c-\frac{3}{2}\bar{\kappa}-\frac{27}{8}\bar{q} & -\frac{\sqrt{3}}{4}(\bar{g}_c+2\bar{\kappa}+\frac{7}{2}\bar{q}) \\ i\sqrt{3}\,T & -\frac{\sqrt{3}}{4}(\bar{g}_c+2\bar{\kappa}+\frac{7}{2}\bar{q}) & -\frac{1}{4}\bar{g}_c-\frac{5}{2}\bar{\kappa}-\frac{41}{8}\bar{q} \end{pmatrix}, \tag{1}$$

$$H_{K2}+H_{\text{exch}}=\frac{\hbar^2K^2}{2m_0}\begin{pmatrix} \gamma_1^{\text{ex}}-2\gamma_2^{\text{ex}} & 0 & 0 \\ 0 & \gamma_1^{\text{ex}}+\gamma_2^{\text{ex}} & -\sqrt{3}\gamma_2^{\text{ex}} \\ 0 & -\sqrt{3}\gamma_2^{\text{ex}} & \gamma_1^{\text{ex}}-\gamma_2^{\text{ex}}+\frac{2m_0}{\hbar^2K^2}E_{T-t} \end{pmatrix}, \tag{2}$$

where

$$\begin{aligned} \bar{g}_c&=\tilde{g}_c\mu_B H\,,\\ \bar{\kappa}&=\tilde{\kappa}\mu_B H\,,\\ \bar{q}&=\tilde{q}\mu_B H\,,\\ T&=9\hbar K_l K m_0/16(\gamma_1 m_e^*+m_0)\,. \end{aligned} \tag{3}$$

The definitions of $(\tilde{g}_c,\tilde{\kappa},\tilde{q})$ and K_l are given in Refs. 3 and 4. By using the Luttinger parameters γ_1 and γ_2 ($\gamma_3=\gamma_2$ is assumed as described before), γ_1^{ex} and γ_2^{ex} are represented by

$$\begin{aligned} \gamma_1^{\text{ex}}&=m_0/(m_e^*+m_0/\gamma_1)\,,\\ \gamma_2^{\text{ex}}&=[m_0/(m_0+m_e^*\gamma_1)]^2\gamma_2\,. \end{aligned} \tag{4}$$

We have neglected a term including $g_3(E)$ (Ref. 10) in Eq. (4), since it is evaluated to be much smaller than other terms. One may notice that $m_0/(\gamma_1^{\text{ex}}-2\gamma_2^{\text{ex}})$ and $m_0/(\gamma_1^{\text{ex}}+2\gamma_2^{\text{ex}})$ are the centers of mass of heavy and light mass excitons, respectively, when E_{T-t} (energy separation between E_T and E_t, see Fig. 6) becomes negligible in comparison with the kinetic energy.

In deriving the block-diagonal forms of (1) from a complete Hamiltonian matrix,[3] we have neglected slight mixings between differently polarized substates due to smaller off-diagonal matrix elements including T and $\bar{q}$. In addition, the anisotropic spin-exchange splitting ($\tilde{\Delta}_2$) is neglected for the reasons described in Ref. 4.

The line-shape fitting of the reflectance spectra has been done according to the newly developed method,[11] which gives a practical way to calculate refractive indices of multicomponent polaritons for a given value of light frequency ω. The polariton dispersions are given by the solution of $\det S=0$, where

$$S=\begin{pmatrix} & & \nu_1 \\ & & \vdots \\ H\left(\frac{n\omega}{c}\right)-\hbar\omega\underline{1} & & \nu_j \\ & & \vdots \\ & & \nu_s \\ \nu_1^*\cdots\nu_j^*\cdots\nu_s^* & & (n^2-\bar{\epsilon}_b)/4\pi \end{pmatrix}. \tag{5}$$

The ν_j is the dipole matrix element from the ground state to the jth exciton basis state chosen for the matrix representation of H. n and $\bar{\epsilon}_b$ in (5) represent cK/ω and the background dielectric constant, respectively. This corresponds to taking only the positive-frequency part of the dielectric function, $\bar{\epsilon}_b$ representing the background effect of all the other (including negative-frequency) oscillators. As the additional boundary conditions, we require that the sum of the jth exciton amplitudes of all the $s+1$ polaritons vanish at the surface for any j ($1\sim s$). This is in a sense an extension of the Pekar-Hopfield-type additional boundary condition (ABC), namely, "the resonant part of polarization should vanish at the surface." If the interaction Hamiltonian is already diagonal, our ABC reduces to Pekar-Hopfield's. The extension was made to include the contribution of spin triplet (dipole-forbidden) excitons. There could be a variety of other ABC's corresponding to different microscopic specifications of surface potential for the motion of excitons. Microscopic derivation of an ABC for multicomponent polaritons is a complex problem and is outside the scope of this paper. The lifetime effect of the exciton is introduced by

putting imaginary parts into the diagonal elements of the Hamiltonian. For the right choice of the set of n's obtained from $\det S=0$, we allowed only the waves decaying toward the inside of the crystals, as required in usual reflectance calculations. This corresponds, for real n's, to taking the branches with positive group velocities (see the Appendix). For the present situation where the Hamiltonian is represented by (1) and (2), we have simply

$$(\nu)=\begin{bmatrix}0\\0\\\nu_1\end{bmatrix}. \tag{6}$$

According to this procedure, a definite line shape of the reflectance spectrum can be calculated for a given set of parameters, some of which are already experimentally evaluated. For the present fit shown below, we employed $4\pi\beta=8\pi\nu_1^2/E_0=2.47\times10^{-2}$, $\bar{\epsilon}_b=6.20$, and $\gamma_1^{ex}=0.59$,[12] where E_0 is the energy of $|J=1,M_J\rangle$ at $K=0$ and $H=0$.

In the first place, the reflectance anomaly at $H=0$ can be reproduced only in the presence of the k-linear term. The polariton dispersion and hence the reflectivity are strongly influenced by the effects of the k-linear term and the heavy and light masses. As for γ_2^{ex} in the numerical calculations, it is varied from zero to $\frac{1}{2}\gamma_1^{ex}$, the limit where the heavy exciton mass becomes infinity. A unique decision of the set of parameters (T, E_{T-t}, and γ_2^{ex}) cannot, however, be made on the basis of the line-shape fitting at $H=0$ alone.

Therefore we try to fit the line shape of magnetoreflectance spectra in the Faraday configuration with $\vec{K}\,||\,\vec{H}\,||\,[110]$. Since the splitting of the σ_{-1} and σ_{+1} components of the reflectance anomaly has been found to be linear in the magnetic-field intensity within the high-field region, we employ a linear Zeeman regime as a starting approximation to analyze the magnetoreflectance spectra. In this regime, the g values for the $|1,\pm1\rangle$ and $|2,\mp2\rangle$ states, polarized for $\sigma_{\pm1}$, respectively, for $\vec{K}\,||\,\vec{H}\,||\,[110]$ are represented by

$$-\tfrac{1}{2}\tilde{g}_c-5\tilde{\kappa}-\tfrac{41}{4}\tilde{q} \tag{7}$$

and

$$-\tilde{g}_c+6\tilde{\kappa}+12\tilde{q}. \tag{8}$$

Assuming $\tilde{q}=0$, as in the case of GaAs, InP (Ref. 2), and CdTe,[5] and putting the evaluated g values $+0.6\pm0.1$ and -1.8 ± 0.1 for (7) and (8), we get

$$\tilde{g}_c=0.68\pm0.15,$$

$$\tilde{\kappa}=-0.19\pm0.02.$$

Figures 6(b), 6(c), and 6(d) show the polarization-resolved magnetoreflectance spectra calculated with the following parameters summarized in Table I: $\tilde{g}_c=0.68$, $\tilde{\kappa}=-0.19$, $\hbar K_l=0.54\times10^{-9}$ eV cm, $E_{T-t}=0.4$ meV, and $\gamma_2^{ex}=0.20$.[13] In this calculation, the presence of the surface dead layer is neglected for simplicity. The remarkable experimental feature that the anomalous spike has a much broader and stronger structure for σ_{-1} polarization than for σ_{+1} at high fields is well reproduced by this model. In Fig. 6(a) is shown the corresponding reflectance spectrum at $H=0$ calculated by using the same parameters in comparison with the experimental spectrum. The qualitative agreement of the reflectance line shape supports the present model for the reflectance anomaly. An inclusion of the surface dead layer would provide a better agreement between the experimental and calculated spectra as shown in a forthcoming paper on CdTe.[5] The longitudinal-transverse splitting of the Γ_5 exciton states is evaluated as $E_{L-T}=6.1$ meV, from which we obtain $-2\tilde{\Delta}_1=2.4$ meV through the relation $E_{T-t}=-2\tilde{\Delta}_1-\frac{1}{3}E_{L-T}$. It should, however, be mentioned that the above values of ($\hbar K_l, E_{T-t}, \gamma_2^{ex}$) are not unique, namely, very similar line shapes can be obtained from different sets of values. Besides, we must consider that the details of measured spectra are also sample dependent. Thus one can at most determine the region of plausible values of the parameters. A general tendency is that $\hbar K_l$ and E_{T-t} get larger for smaller γ_2^{ex}.

We discuss next the result of magnetoreflectance

TABLE I. Exciton and band parameters evaluated in the present work.

E_{L-T}	6.1 meV
E_{T-t}	0.4 meV
$-2\tilde{\Delta}_1$	2.4 meV
$\tilde{\Delta}_2$	0
$4\pi\beta$	2.47×10^{-2}
$\bar{\epsilon}_b$	6.20
γ_1^{ex}	0.59 (Ref. 12)
γ_2^{ex}	0.20 (Ref. 13)
g (broad reflectance, Faraday [a])	$+0.6\pm0.1$
g (reflectance spike, Faraday [a])	-1.8 ± 0.1
g (reflectance spike, σ in Voigt [a])	0.9 ± 0.1
$\tilde{g}_c$	0.68 ± 0.15
$\tilde{\kappa}$	-0.19 ± 0.02
$\tilde{q}$	0
$\hbar K_l$	0.54×10^{-9} eV cm

[a] See text for details.

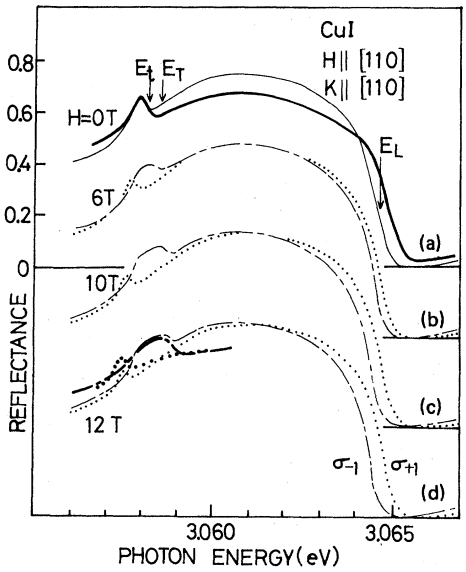

FIG. 6. Reflectance spectra of the $Z_{1,2}$ exciton polaritons in CuI calculated for $\vec{K}||\vec{H}||[110]$. The exciton resonance energies at K = 0 are given by $E_t(\Gamma_{3,4})$, $E_T(\Gamma_5$ transverse), and $E_L(\Gamma_5$ longitudinal). The parameters employed are $\tilde{\epsilon}_b = 6.20$, $\Sigma_t 4\pi\beta_t = 2.47\times10^{-2}$, $E_{T-t} = 0.4$ meV, $\tilde{\Delta}_2 = 0$, $\tilde{g}_c = 0.68$, $\tilde{\kappa} = -0.19$, $\tilde{q} = 0$, $\hbar K_t = 0.54\times10^{-9}$ eV cm, $\gamma_1^{ex} = 0.59$, and $\gamma_2^{ex} = 0.2$. As a damping parameter, $\Gamma = 0.17$ meV is employed where 2Γ gives the full half-width. The thick curves show the corresponding experimental spectra for comparison. The absolute magnitude of the measured reflectivity is taken arbitrarily, since it is not accurately calibrated.

in the Voigt configuration with $\vec{K}||[110]$ and $\vec{H}||[1\bar{1}0]$. Though the details of the k-linear term mixing scheme in this configuration are described in the Appendix of the second paper of Ref. 3, we repeat here an important result about the selection rules in the magnetic field. Contrary to the result in the Faraday configuration with $\vec{K}||\vec{H}||[110]$, $|2,\pm1\rangle$ states are strongly coupled with $|1,\pm1\rangle$ states and become observable as a reflectance anomaly in this Voigt configuration due to the off-diagonal k-linear terms. Employing here the linear Zeeman regime again, the splitting of the two σ components is given by

$$|\tfrac{1}{2}\bar{g}_c - 3\bar{\kappa} - \tfrac{27}{4}\bar{q}|. \qquad (9)$$

Putting $\tilde{q} = 0$, $\tilde{g}_c = 0.68$, and $\tilde{\kappa} = -0.19$ evaluated from the magnetoreflectance in the Faraday configuration, we obtain a corresponding g value for this splitting of 0.91 which is consistent with the experimental value of 0.9 ± 0.1. This result gives validity to the assumption that $\tilde{q}$ is negligible in the present case. Meanwhile, the appearance of the longitudinal exciton state Γ_{5L} in the σ spectrum is attributed to a linear Zeeman mixing with the Γ_{5T} state. The corresponding off-diagonal matrix element is given by $-ig_5H$ (Ref. 3) which is represented by $-i(-\frac{1}{4}\bar{g}_c - \frac{5}{2}\bar{\kappa} - \frac{41}{8}\bar{q})$. Then this Zeeman energy is evaluated as 0.21 meV at $H = 12$ T by using the above-employed values of $\tilde{g}_c$, $\tilde{\kappa}$, and $\tilde{q}$. In accordance with the appearance of the $L-T$ mixed mode, the energy position of the upper polariton edge is shifted approximately by the amount of $|-ig_5H|$ provided the original longitudinal-transverse splitting is much larger than this energy. The energy shift of the upper polariton edge as 0.18 ± 0.02 meV estimated from the spectra in Fig. 3 is in reasonable agreement with this value of $|-ig_5H| = 0.21$ meV.

B. Polariton luminescence under a magnetic field

We start from a simple picture of polaritons for the $Z_{1,2}$ exciton luminescence neglecting the effects of the k-linear term and the light and heavy masses. Then we have only two polariton branches, upper and lower polariton states, associated with the Γ_{5T} exciton state[7] at $H = 0$, each of which is expected to split under a magnetic field. For $H \neq 0$, the contribution of the polaritons associated with the $|2,\pm1\rangle$ excitons to the luminescence is neglected for the moment, since the off-diagonal linear Zeeman energy between $|2,\pm1\rangle$ and $|1,\pm1\rangle$ is much smaller than E_{T-t} even at $H = 10$ T, according to the preceding discussions. The luminescence band UP at 3.065 eV is considered first. The coincidences of the g value of this luminescence band $(+0.7\pm0.1)$ with that of the Γ_{5T} reflectance band $(+0.6\pm0.1)$ and the energy position of the luminescence peak with E_L enable one to assign the UP band to the upper polariton luminescence. Meanwhile, the lower polariton luminescence band associated with the Γ_{5T} exciton state is expected to be observed with the same g value as the upper polariton luminescence if the contribution of the polaritons associated with $|2,M_J\rangle$ is properly subtracted. Judging from the qualitative resemblance of the background MCP between 3.054 and 3.060 eV shown in Figs. 4 and 5 to the MCP spectra of the upper polariton luminescence, one is tempted to assign the background MCP spectra to the lower polariton luminescence band associated with the Γ_{5T} exciton state. In order to check this possibility, the background MCP spectra are inversely transformed to the luminescence spectra by assuming rigid shifts corresponding to the g value of +0.7. One of the results at $T = 55$ K and $H = 10$ T is represented in Fig. 5 by the dotted line. Most parts of the luminescence intensity between 3.054 and 3.060 eV are reproduced by the thus calculated luminescence spectrum, which provides good support to the idea that the lower polariton luminescence originating from the Γ_{5T} exciton state produces the background of the MCP spectra.

With respect to the unusual temperature change of the MCP spectra, the bound exciton is playing the leading role: In accordance with the decrease of temperature, the intensity of the bound exciton luminescence increases, and the corresponding MCP signal makes the background MCP due to lower polariton state less pronounced at low temperatures.

Now we take the effect due to the finite exciton wave vector into consideration. Both exciton and polariton dispersion curves with infinite lifetime are calculated for $\vec{K}\|[110]$ in Fig. 7 by using the exciton and band parameters estimated from the reflectance line-shape analysis (see Table I). Since the dispersion curve obtained from (1), (2), and (5) is symmetric with respect to the change of the sign of the wave vector, only the dispersion in the positive K region is shown in Fig. 7 for simplicity. One should take the portion of the polariton curves with $dE/dK>0$ or $dE/dK<0$ within the whole K region depending upon the situation under consideration (reflectance or luminescence). For excitons with a small finite lifetime, the portion of the dispersion curve with positive (negative) group velocity corresponds to the refractive index with the positive (negative) imaginary part (see the Appendix). The corresponding relative oscillator strength of each exciton state is given in Fig. 8 as a function of the wave vector $\vec{K}$ in the [110] direction. Here the six exciton states become dipole allowed at $K\neq 0$, as seen from Eqs. (1) and (2).

Each of the three exciton states given in Fig. 7(a) is twofold degenerate because of the zero Zeeman energy at $H=0$. Although four polariton branches are composed from these three exciton states, the upper polariton branch is not discussed further because it is much less influenced by the k-linear term effect. The energy splitting between the 1 and 2 exciton states is almost linear in K at small K as shown in Fig. 7(a), which is an important feature of this effect. A clamping of the 2 and 3 exciton states at around $K=1.7\times10^{6}\ \mathrm{cm}^{-1}$ is well described by Fig. 8(a) which yields characteristic dispersions of the II and III polaritons. Judging from the half-width (about 2 or 3 meV) of the corresponding luminescence band, all of the I, II, and III branch polaritons can be contributing to the observed luminescence. One notices, however, that the corresponding luminescence spectrum does not show fine structures. There may be several reasons accounting for this fact, such as finite lifetime of each polariton state, finite angular or wave-vector divergence of the luminescence light accepted by the detector, or limited resolution of the monochromator. In particular, the overlap of three polariton luminescence bands, each of which

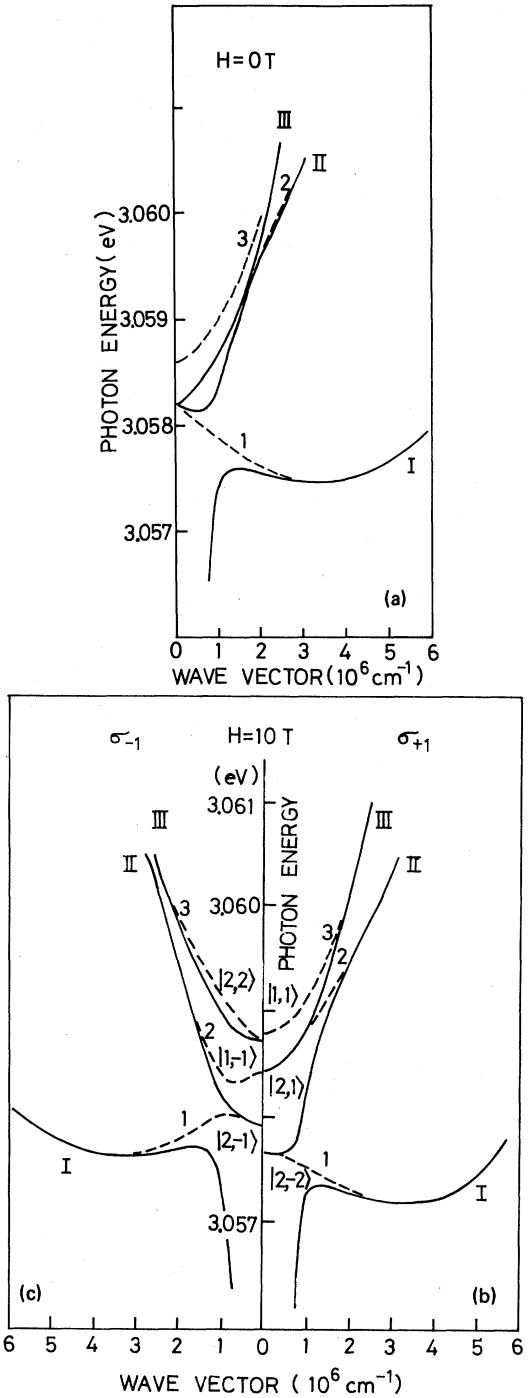

FIG. 7. Polariton dispersion curves (solid) as well as the exciton dispersion curves (dashed) at (a) $H=0$ T and (b) and (c) $H=10$ T for $\vec{K}\|\vec{H}\|[110]$ calculated for the parameters employed in Fig. 6 except that zero damping is employed for convenience. The leading exciton components at $K=0$ are given by $|J,M_J\rangle$. The polariton branches and exciton branches are named I, II, and III and 1, 2, and 3, respectively, from the low-energy side. The dispersion curve due to the upper-branch polariton (UP) is off scale in this figure.

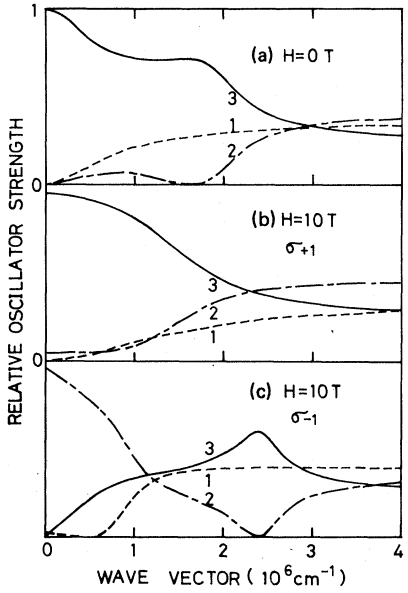

FIG. 8. Relative oscillator strength of each exciton state given in Fig. 7 as a function of wave vector.

has considerable bandwidth resulting from its distribution on the dispersion curve, may be playing an essential role. Even though the structures of the luminescence band are thus obscured, there is a chance to trace them by modulation spectroscopy. The MCP at $H \neq 0$ really enabled us to detect the fine structures of the luminescence band predicted by the polariton model described in Fig. 7.

We consider now the situation that the exciton-polaritons influenced by the effect due to a finite exciton wave vector further interact with one another under magnetic fields. The dispersion curves of excitons and polaritons are calculated in Figs. 7(b) and 7(c) for the parameters evaluated before. The leading component of each exciton branch at $K=0$ is given by $|J, M_J\rangle$ in these figures. The magnitudes of the linear Zeeman mixing between $|1, \pm 1\rangle$ and $|2, \pm 1\rangle$ states are manifested in the relative oscillator strength of the exciton 2 for σ_{+1} and of exciton 1 for σ_{-1} at $K=0$ in Fig. 8. One notices from Figs. 7(b) and 7(c) that the orderings of the Zeeman components ($|1, \pm 1\rangle$ as well as $|2, 2\rangle$, $|2, 1\rangle$, $|2, -1\rangle$, and $|2, -2\rangle$) are normal and characterized by positive g values. Therefore the negative g value experimentally observed for the reflectance anomally can be only explicable by the k-linear term effect which induces the $|2, -2\rangle$ ($|2, +2\rangle$) state allowed for σ_{+1} (σ_{-1}) polarization.

Returning to the MCP spectra, we remember that the two additional structures observed besides the background and bound exciton MCP have negative g values. On the basis of the polariton scheme shown in Fig. 7, these MCP structures are qualitatively interpreted as follows.

In the first place, the MCP structure at around 3.059 eV (Fig. 4) can be assigned as originating from the difference of these luminescence bands to the III polaritons in σ_{+1} and σ_{-1} polarization. In this polariton branch, the bottom part below the clamping energy is characterized mainly by $|2, 1\rangle$ in σ_{+1} and $|2, 2\rangle$ in σ_{-1}. Therefore a negative g value is expected for this MCP structure. In the next place, the bottom part of the II polariton branch and the bottleneck part of the I polariton branch are positioned at lower energies for σ_{+1} than for σ_{-1}. The MCP structure with a negative g value at around 3.0575 eV (Fig. 4) can be assigned to the gross difference of these luminescence bands between σ_{+1} and σ_{-1} polarization. With the present resolution, however, it is difficult to separate the contribution from the I and II polaritons. As for the background MCP structure with the positive g value, it has been assigned to the lower polaritons resulting from the $|1, \pm 1\rangle$ exciton states by neglecting the k-linear term effect. Since the oscillator strengths of the $|1, \pm 1\rangle$ excitons are really distributed within the 1, 2, and 3 exciton states to considerable extent as shown in Figs. 8(b) and 8(c), the background MCP should be more properly interpreted as originating from the superimposed contribution from the I, II, and III polaritons. Detailed study of polariton dynamics in this system will be an interesting subject for future research.

ACKNOWLEDGMENTS

The authors are grateful to Professor M. Cardona for supporting the research. Two of us (S.S. and K.C.) would like to thank Max-Planck-Institut für Festkörperforschung for providing guest positions and hospitality during their stay.

APPENDIX

In the text we mentioned the way to choose the appropriate set of polariton wave number K from the solutions of the polynomial equation for K^2 obtained from $\det(S)=0$. The principle of choosing K with positive imaginary part is easy to understand. But the other statement that, for real K, we should take the part of the positive group velocity will need some explanation.

Suppose we have a real solution $\omega(K)$ of the equation

$$c^2K^2/\omega^2 = \epsilon(K, \omega)\,, \tag{A1}$$

which is equivalent to $\det(S)=0$.[11] Around an arbitrary point (K_0, ω_0) on this branch, we may expand $\omega(K)$ as

$$\omega = \omega_0 + v_g(K - K_0) + \cdots\,, \tag{A2}$$

where

$$v_g = \left.\frac{d\omega}{dK}\right|_{K_0} \tag{A3}$$

is the group velocity of the polariton at the point. In order to find the appropriate K in the real (K,ω) plane, we add a lifetime effect to Eq. (A1) and use the principle of positive imaginary part of K. Finally we take the limit of infinitesimal lifetime broadening. Thus our problem is reduced to the following: What part of the dispersion curve in the real plane is obtained from the complex branch with the positive imaginary part by the above-mentioned limiting procedure?

The effect of infinitesimal lifetime broadening in Eq. (A1) is described by changing real ω to a complex $\omega + i0^+$. The analytic continuation of the function $\omega(K)$ has the same expansion (A2) in the complex (K,ω) plane. Hence we have

$$\mathrm{Im}(K) = \mathrm{Im}(\omega)/v_g \ , \tag{A4}$$

namely, a positive $\mathrm{Im}(K)$ for $\omega + i0^+$ can be obtained only for $v_g > 0$. Thus we get our criterion: A propagating mode, which decays in the propagation direction in the presence of lifetime effect, approaches that part of the dispersion curve with positive group velocity in the limit of infinitesimal lifetime broadening.

Applying this principle to the case of Fig. 7(a), for example, we get the allowed portions of the polariton wave numbers $K_j(\omega)$ $(j=1,2,3,4)$, as shown in Fig. 9 by thick lines. Since there are a pair of complex roots, $k_0 \pm ik_1$, of Eq. (A1) on the lower (higher) ω side of each minimum (maximum) of the dispersion curve on the real plane, our choice is the only way to keep the continuity of $K_j(\omega)$ through the extremum points.

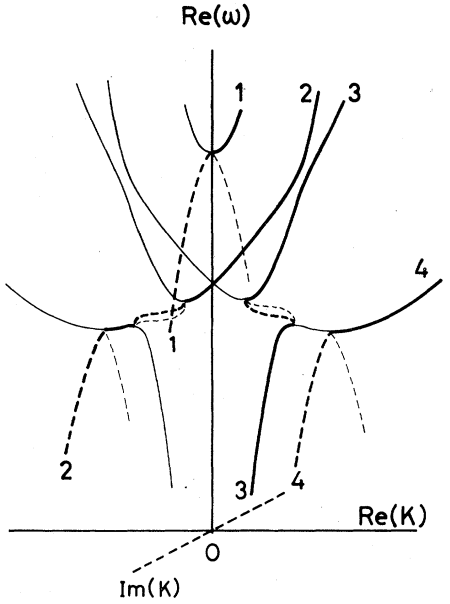

FIG. 9. Schematic representation of the allowed wave numbers $K_j(\omega)$ $(j=1,2,3,4)$, in the case of Fig. 7(a). Thick (solid and dashed) lines are the parts to be adopted. The thick (thin) dashed lines are the solutions with finite positive (negative) imaginary parts.

We are grateful to Professor A. Yoshimori for a useful discussion about this appendix.

[1] A comprehensive review is given by K. Cho, in *Excitons*, edited by K. Cho (Springer, Heidelberg, 1979), Chap. 2.

[2] F. Willmann, S. Suga, W. Dreybrodt, and K. Cho, Solid State Commun. 14, 783 (1974).

[3] K. Cho, S. Suga, W. Dreybrodt, and F. Willmann, Phys. Rev. B 11, 1512 (1975); 12, 1608(E) (1975); K. Cho, *ibid.* 14, 4463 (1976).

[4] S. Suga, K. Cho, and M. Bettini, Phys. Rev. B 13, 943 (1976).

[5] K. Cho, W. Dreybrodt, P. Hiesinger, S. Suga, and F. Willmann, *Proceedings of the Twelfth International Conference on the Physics of Semiconductors*, edited by M. H. Pilkuhn (Teubner, Stuttgart, 1974), p. 945; W. Dreybrodt, K. Cho, S. Suga, F. Willmann, and Y. Niji, Phys. Rev. B 21, 4692 (1980).

[6] C. Schwab, J. Ringeissen, R. Heimburger, and S. Nikitine, J. Chem. Phys. 65, 1035 (1968).

[7] S. Suga, K. Cho, P. Hiesinger, and T. Koda, J. Lumin. 12/13, 109 (1976).

[8] W. Staude, Phys. Status Solidi B 43, 367 (1971).

[9] J. J. Hopfield and D. G. Thomas, Phys. Rev. 132, 42 (1963).

[10] E. O. Kane, Phys. Rev. B 11, 3850 (1975).

[11] K. Cho, Solid State Commun. 27, 305 (1978).

[12] C. I. Yu, T. Goto, and M. Ueta, J. Phys. Soc. Jpn. 34, 693 (1973). Since $m_e^* \sim 0.3$ and $m_h^* \sim 1.4$ are evaluated on the basis of hydrogenic exciton series, γ_1 can be estimated as 0.7. Thus we employed $\gamma_1^{\mathrm{ex}} = 0.59$ tentatively for the following analysis.

[13] This value corresponds to $\gamma_2 = 0.29$ according to Eq. (4). In the case of CuBr, H. J. Mattausch and Ch. Uihlein have evaluated Luttinger parameters γ_1, γ_2, and γ_3 in Solid State Commun. 25, 447 (1978).